# Localized surface-plasmon resonances and negative refractive index in nanostructured electromagnetic metamaterials

J. Parsons, E. Hendry, J. R. Sambles, and W. L. Barnes
*School of Physics, University of Exeter, Stocker Road, Exeter EX4 4QL, United Kingdom*
(Received 12 October 2009; published 23 December 2009)

We explore the extent to which the concept of localized surface-plasmon resonances can be used to explain the optical response of complementary electromagnetic metamaterials in the visible. The two complementary metallic nanostructures investigated are the mesh-based and particle-based structures, more specifically stacked periodic arrays of particles and stacked periodic arrays of holes in metallic sheets. Using finite-element modeling we show how hybridization of the localized surface-plasmon resonances associated with individual nanostructures (particle and hole) can be used to help understand the optical response of these materials. In particular, we look at the electromagnetic field distributions and the effective permittivity and permeability.

DOI: 10.1103/PhysRevB.80.245117 PACS number(s): 73.20.Mf, 78.20.Bh, 78.20.Ci, 42.25.Bs

## I. INTRODUCTION

The term "negative index" was first used by Veselago[1] to describe materials which possessed both a negative (electric) permittivity and a negative (magnetic) permeability. Optical materials that simultaneously have a negative permittivity and permeability do not naturally occur. However, in the past few years there has been an explosion of interest in electromagnetic metamaterials. These artificial materials, which are structured on length scales shorter than the wavelength of the light involved, can have properties far from those of the constituent materials,[2,3] including a negative refractive index.[4]

A key idea behind electromagnetic metamaterials is that they allow the electric *and* the magnetic fields of the incident light to interact with the material, thereby enabling a much richer range of phenomena to be observed than has been traditional in optics. Metals are naturally occurring materials that have a negative permittivity, with which the electric field may interact strongly at optical frequencies. However, there are no naturally occurring materials with which the magnetic field may interact strongly at optical frequencies. Instead, a number of different structural elements have been developed that allow electromagnetic metamaterials to exhibit the desired magnetic response. These structures include split-ring resonators,[4] cut wire pairs and pairs of plates,[5–7] and meshed structures such as the "fish scale"[8] and "fishnet."[9] A negative index of refraction may be observed for a material which interacts simultaneously with both the electric-field and magnetic-field components of the incident radiation. Experimental verification of a metamaterial with a negative index of refraction was first performed in the gigahertz frequency regime using a three-dimensional arrangement of copper wires and split rings.[4] The negative index behavior has been explained through analogy with inductive and capacitive elements in an electrical circuit.[10] More recently, an exciting advance has been the development of near infrared/visible frequency negative index metamaterials, which are engineered by perforating a stacked arrangement of metallic and dielectric layers with subwavelength holes to create a fishnet-type structure.[11,12]

For the present study two classes of design are of particular interest, one based on arrays of short metallic wires (particles) and the other based on arrays of holes in metal sheets, so-called fishnet structures. From a geometric perspective the particle-array and hole-array structures appear complementary. Furthermore, both metallic nanoparticles and nanoholes in metallic sheets support localized surface-plasmon resonances (LSPRs). For stacked arrays of metallic nanoparticles, an interesting alternative to the electric circuit analogy has been developed,[13] one that considers the LSPRs associated with individual metallic nanostructures.[14,15] In particular, this view looks at the importance of the hybridization of these localized modes when neighboring elements interact.[13] It is well established that metallic nanoholes support LSPRs in much the same way as nanoparticles.[16–19] Can one understand the behavior of the fishnet structures from the same perspective? This is the question explored here. We have considered structures that are not ideal in terms of providing a negative refractive index but are instead chosen to facilitate the comparison of complementary structures.

Utilizing finite-element numerical modeling, it is shown that stacked layers of both hole and particle arrays have resonances at similar frequencies, giving rise to both electric (permittivity) and magnetic (permeability) responses. For appropriately designed hole-array structures, the frequency of the magnetic resonance coincides with a region of negative effective permittivity and a negative index of refraction is seen in the simulation. In contrast, in our complementary stacked particle arrangement no such negative index is found. The absence of a region of negative index can be explained through the effective permittivity being positive rather than negative, something which is primarily a consequence of the low filling fraction of metal in the chosen structure.

## II. NUMERICAL SIMULATIONS

Numerical simulations were performed using a commercial finite-element package (ANSOFT HFSS version 11.0) with a mesh size of 4.0 nm. Permittivity values for silver were taken from reference data.[20] We compared complementary two-dimensional (2D) arrays of cylindrical holes (curve A) and cylindrical particles (curve B) formed from a silver film with thickness 20 nm. For each of the structures, the hole/

 

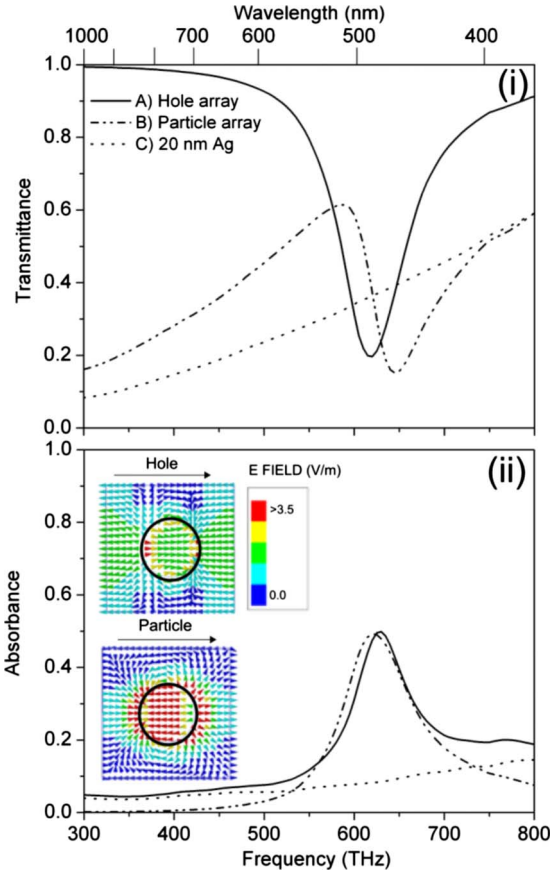


FIG. 1. (Color online) Simulated (i) transmittance and (ii) absorbance spectra are shown for (A) an infinite array of 90 nm diameter holes in a 20-nm-thick Ag film with period 225 nm, (B) an infinite array of 90 nm diameter, 20 nm height cylindrical Ag particles with period 225 nm, and (C) a 20-nm-thick continuous Ag film. In all simulations the structures were illuminated at normal incidence in vacuum. The inset of (ii) shows the instantaneous scattered electric-field distributions at the resonant frequency, for a cross section in the plane of the array, through the center of the hole-array and particle-array structures. Both distributions are shown at the same instant in phase for radiation incident with frequency $6.25\times10^{14}$ Hz ($\lambda_{vac}$=480 nm). The arrows above the field distributions indicate the direction of the incident electric-field vector.

particle diameter was 90 nm and the period of the square array was 225 nm. Choosing the same hole and particle diameters and the same array periods is not enough to ensure the resonances of the two complementary types of structure are the same. The parameters we have used here were selected so as to ensure hole and particle resonances occurred at similar frequencies.[18] A more extensive discussion comparing hole and particle arrays in the nondiffracting regime (for frequencies in the vicinity of LSPRs) has been published elsewhere.[18]

## III. RESULTS AND DISCUSSION

### A. Monolayer particle and hole arrays

In Fig. 1, the simulated transmittance and absorbance spectra are compared for complementary 2D arrays of cylindrical holes (curve A) and cylindrical particles (curve B) formed from a Ag film with thickness 20 nm. In both hole and particle arrays, distinct transmittance minima are observed at ~490 nm which are accompanied by absorbance maxima. In our hole-array and particle-array structures, the period of the array has been chosen such that the structure is zeroth order for frequencies in the vicinity of LSPRs. For the hole arrays, we therefore do not expect any coupling of incident radiation to surface plasmon-polariton modes associated with the metal film.[21] The absorbance maxima in both particle-array and hole-array structures are attributed to the coupling of incident radiation to LSPR modes associated with the charge distributions which are induced across the metallic nanoparticle and in the vicinity of the nanoholes in the metallic film. Additional numerical simulations (not shown) indicate that the LSPRs associated with an individual hole-array layer are independent of the angle of incidence, demonstrating that the mode is not diffractively coupled and is localized in nature. A significant point to note is that while particle and hole LSPRs occur at similar frequencies, their field distributions show important differences. The inset in Fig. 1(ii) shows the instantaneous scattered electric field at the resonant frequency, for a cross section normal to the plane of incidence through the center of the hole-array and particle-array structures. The scattered electric field within the hole and within the particle oscillate out of phase with respect to each other when referenced to the phase of the incident electric field. The scattered fields are shown for the same phase of the incident wave and indicate that the field distributions within the region occupied by the hole/particle are complementary. Furthermore, for the hole array, in addition to there being significant field enhancement within the hole, enhancement is also observed in the metallic regions between holes, something which is absent for the vacuum regions of the complementary particle-array structure. This enhanced field between the holes is a feature of the coupling between the induced dipole moments associated with neighboring holes.

### B. Bilayer arrays

Previously it has been shown that when structures exhibiting LSPRs are placed in close proximity,[22,23] the modes they support may interact or couple, so as to modify the resonant frequency and line shape. When our 2D LSPR arrays are modified by the addition of further arrays (see Figs. 2 and 5), hole and particle LSPRs in adjacent layers hybridize, resulting in splitting of the single-layer LSPR resonances. Similar to the monolayer arrays discussed in the previous section, numerical simulations (not shown) indicate that the coupled LSPRs of the multilayer structures are independent of the angle of incidence and are therefore localized in nature. In order for significant interaction between layers to occur, the layer spacing must be comparable or less than the decay length of the localized field associated with the LSPR,[24] just as for planar films.[25–27] In Fig. 2, grayscale plots show the simulated absorbance as a function of frequency and layer spacing for (i) two-hole-array layers and

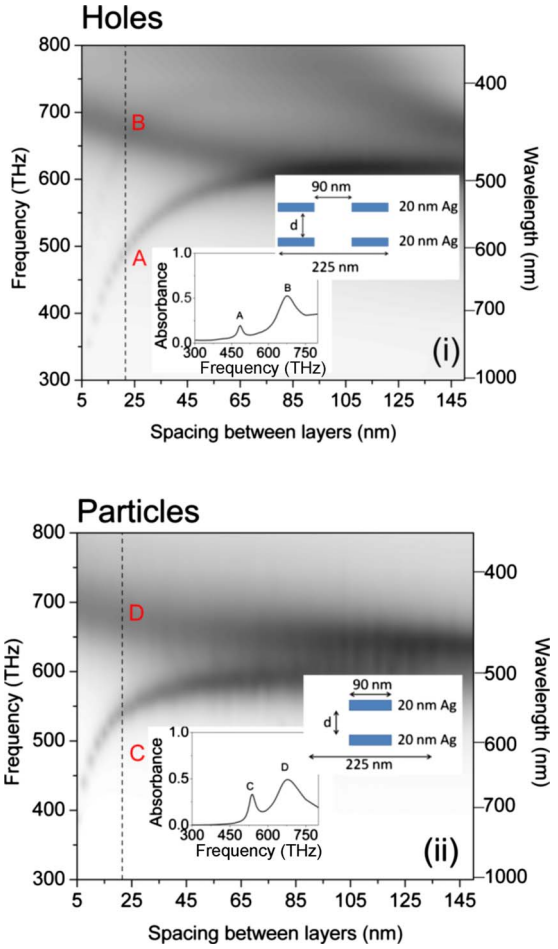


FIG. 2. (Color online) The simulated absorbance is plotted as a function of frequency and spacing between two layers of (i) hole and (ii) particle arrays. Dark regions correspond to significant absorption and are indicative of the coupling of incident light to modes of the double-layer structure. In both structures the Ag layer thickness is 20 nm and cylindrical holes/particles with diameter 90 nm are arranged into regular square arrays with period 225 nm. For 20 nm layer spacing (shown by the dashed line), the absorbance for each arrangement is plotted as a function of frequency as an inset figure.

(ii) two-particle-array layers, both types of array having the same parameters as the single-layer structures shown in Fig. 1. As the spacing between the layers is decreased, particularly below 60 nm, a distinct splitting is observed in the LSPR associated with the response of the single-layer structure: two resonant modes are observed, one is blueshifted to frequencies above that of the single-particle LSPR while the other mode is redshifted. For the double particle array, Fig. 2(ii), the modes still appear to be split at separations up to 150 nm. Further modeling (not shown) indicates that the splitting is reduced as the layer spacing is further increased, the splitting disappearing for separations of more than 200 nm.

The insets in Fig. 2 show the absorbance plotted as a function of frequency for two-layer structures comprised of (i) hole arrays and (ii) particle arrays with a fixed layer spacing of 20 nm. Again, two clear maxima are evident, labeled

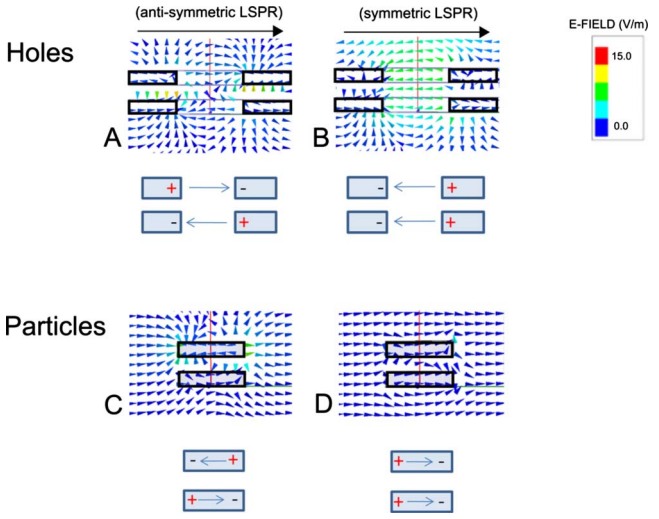


FIG. 3. (Color online) The instantaneous scattered electric-field vector is shown at the asymmetric (A and C in Fig. 2) and symmetric (B and D in Fig. 2) resonant frequencies for a vertical cross section through two complementary hole (upper) and particle (lower) array layers separated by 20 nm. All distributions are shown for the same phase of the incident field and are taken for a cross section which is perpendicular to the plane of the arrays and parallel to the plane of incidence. The arrows above the field profiles indicate the direction of the incident electric-field vector.

A and B for the hole-array, and C and D for the particle-array structures, respectively. Christ *et al.*[13] have previously observed this hybridization of LSPRs for particles spaced by a few tens of nanometer in array structures. Notice that for both particle-based and hole-based structures the lower frequency resonances are both weaker and narrower than the higher frequency resonances, see absorbance insets in Figs. 2(i) and (ii). The relative weakness and narrowness arises from the asymmetric nature of the low-frequency mode (see below): the charge distribution of such modes mean that they are only weakly coupled to radiation; the radiative damping is thus significantly less than for the symmetric resonance.

The field distributions at the resonant frequencies are plotted in Fig. 3. All distributions are shown at the same phase of the incident field and are taken for a cross section which is perpendicular to the plane of the arrays, parallel to the plane of incidence. The black arrows at the top of the figure denote the direction of the incident electric field. At resonance B (the high-frequency branch of the coupled LSPR for the hole structure) the fields inside adjacent holes are aligned, suggesting a symmetric distribution of charges associated with the coupled LSPRs in the upper and lower layers. In contrast, the fields associated with resonance A (the low-frequency branch) are out of phase and suggest an asymmetric charge distribution. A similar relationship is observed for the two-layer particle structures. For the symmetric resonances (B and D), the aligned nature of the electric dipole moments in adjacent layers increases the dipolar restoring force associated with the resonance, thus giving rise to a greater resonant frequency than would be expected for a single layer. For the asymmetric resonances (A and C), the electric dipole moments in adjacent layers are in opposite directions and the

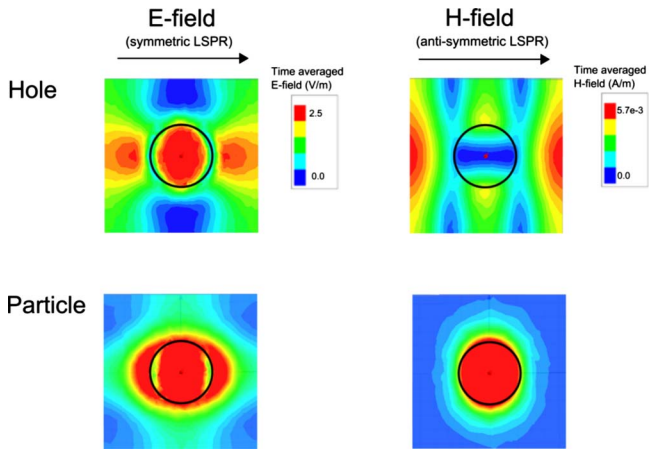


FIG. 4. (Color online) The time-averaged scattered electric-field and scattered magnetic-field distributions are shown for a cross section through the *XY* plane that lies midway between the two layers of hole (left) and particle (right) arrays separated by 20 nm. The arrows above the field profiles indicate the direction of the incident-field vector and the circles denote the positions of the holes/particles which are located above and below the *XY* plane considered here.

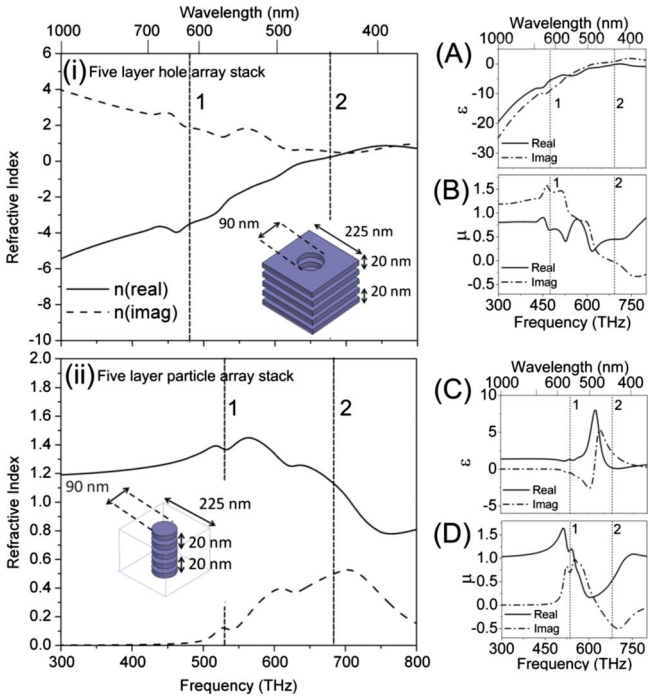


FIG. 5. (Color online) The effective refractive indices are shown as a function of frequency for the five-layer stacked (i) hole-array and (ii) particle-array structures. In the inset, the real and imaginary parts of the effective permittivity ($\varepsilon$) and permeability ($\mu$) are shown for the stacked hole-array (A and B) and particle-array (C and D) structures. The dashed vertical lines in plots (i) and (ii) indicate the resonant frequencies of the asymmetric (1) and symmetric (2) coupled LSPRs for the two-layer structure studied in Fig. 2.

dipolar restoring force will therefore be reduced, leading to a reduction in the resonant frequency when compared to a single-layer structure.[13]

In addition to there being marked differences between the resonant frequencies and line shapes of the symmetric and asymmetric modes, the manner in which incident radiation couples to each mode is also different. The field distributions of the symmetric modes in Figs. 3(B) and 3(D) allow one to see that the electric fields in both the upper and lower layers oscillate in phase. The dipolar nature of the symmetric resonance means that it is easily excited by the incident electric field. In contrast, the incident electric field is not able to couple to the asymmetric resonance. The change in phase of the incident field that occurs over the distance that separates the two layers is much less than the $\pi$ phase change needed to excite this mode. In order for the currents in both layers to be driven out of phase, a separation of approximately $\lambda/2$ would be required, far greater than that used here. Instead, the excitation of the asymmetric mode of the stacked hole-array and particle-array structures occurs through the incident magnetic field. The direction of the incident magnetic field lies in the plane of the arrays, thereby allowing the time-varying incident magnetic field to induce currents in both the upper and lower layers of the hole and particle arrays, the currents in upper and lower layers being in antiphase. Since coupling to the asymmetric mode is achieved using a time-varying magnetic field, the response of the structure is often referred to as a magnetic response.[28] Figure 4 shows the time-averaged field distributions for the symmetric and asymmetric resonances in a plane parallel to the array and midway between the two layers of the hole and particle arrays, which are separated by 20 nm. For the asymmetric resonance, it is seen that there is significant magnetic-field enhancement in the vacuum regions between particles, whereas for the stacked hole arrays the magnetic-field enhancement is not directly under the holes, but instead between holes, as previously noted.[29]

### C. Multilayer arrays

To approach the response expected from a bulk material, we can add further layers to the bilayer structures considered above. We expect five layers of our structure to provide a reasonable approximation to the bulk metamaterial response.[30] Here we consider the optical response of five-layer structures by calculating the real and imaginary components of the effective permittivity, effective permeability, and the effective refractive indices. These effective parameters are determined from the complex reflection and transmission coefficients of the stacked hole-array and particle-array structures, following the procedure of Smith *et al.*[31] In Fig. 5, the real and imaginary parts of the effective refractive indices are plotted (i) for the five-layer stacked hole array and (ii) for the five-layer stacked particle array, the structures have the arrangement shown in the insets. The corresponding complex effective permittivity ($\varepsilon$) and permeability ($\mu$) for the structures are also plotted in (A–D) of Fig. 5.

Both particle and hole structures show resonances in the effective permeability near the frequency of the asymmetric LSPRs exhibited by the two-layer structures, see Fig. 2. These occur at a wavelength of approximately 550 nm for

the particle array and 605 nm for the hole array. We see, however, that the effective permittivities of the structures are dramatically different. In the hole-array structure, a large negative real part of the effective permittivity is observed at low frequencies due to the continuous nature of the metallic layers (i.e., $\varepsilon_r \to -\infty$ in the low-frequency limit) and tends to unity at high frequencies well above the symmetric LSPR. The low-frequency limit for the real part of the effective permittivity of the particles is unity and only falls close to zero in a small frequency region *above* the symmetric LSPR. Further calculations (not shown) indicate that the real part of the effective permittivity becomes negative in this region as the filling fraction of the particle array is increased.

Despite their complimentary nature, particle and hole arrays exhibit very different effective refractive indices. The stacked particle-array structure shows a positive real part of the effective index of refraction across the entire frequency range considered, Fig. 5. In contrast, it can be seen that the stacked hole-array structure exhibits a wide frequency region in which the real component of the effective index of refraction is negative. The hole-array structure is an example of a "single-negative" negative index metamaterial.[5,7,32] Others have shown that the real part of the index of refraction can be negative in a material for which the real parts of the effective permittivity and permeability are not simultaneously negative, provided that the condition $\mu_r\varepsilon_i + \varepsilon_i\mu_r < 0$ is satisfied.[33] The region of negative index in our stacked hole-array structure occurs when $\mu_r$ and $\mu_i$ are both positive and both $\varepsilon_r$ and $\varepsilon_i$ are large and negative. The appearance of a negative imaginary part of the effective permittivity may at first seem rather strange but it is a consequence of the dispersive nature of the electric and magnetic resonances.[34] At this point, it should be noted that by changing the structural parameters of the stack (i.e., larger holes and larger pitch) and/or introducing a high index dielectric, the frequency of the asymmetric LSPR will shift to lower frequency, pulling the negative index region from the visible into the infrared.[11]

In contrast to the hole-array structure, our stacked particle-array structure does not exhibit a region of negative refractive index. A negative index would require the real component of the effective permittivity to be negative in the region of the asymmetric LSPR (the magnetic resonance). However the discontinuous nature of the metal in the particle-array structure leads to the real component of the effective permittivity being positive rather than negative. Others have looked at how particlelike (wire and plate) structures may be engineered to improve their response to try to achieve a negative effective permittivity at frequencies up to the visible.[6,35,36] To the best of our knowledge, a negative index of refraction at visible wavelengths (400–750 nm) has not yet been achieved using a discontinuous metallic metamaterial.

## IV. CONCLUSION

An alternative explanation to the commonly used electrical circuit formalism for characterizing the optical response of negative index metamaterials has been pursued. We have explored how the optical response of both stacked hole-array and stacked particle-array structures can be explained in terms of localized surface-plasmon resonances. The interaction between resonances in adjacent layers leads to symmetric and asymmetric coupled modes. In both stacked particle-array and stacked hole-array structures, the symmetric coupling of LSPRs of adjacent particles/holes on different layers yields an electric response. For the stacked hole arrays, the symmetrically coupled LSPRs lead to a modest perturbation to the real part of the effective permittivity from that of a bulk metal. In contrast, the symmetrically coupled LSPR of the particle array provides the only deviation from unity in effective permittivity. The asymmetrically coupled LSPRs are responsible for the magnetic response in both stacked hole and particle arrays. Unlike the stacked particle array, the magnetic-field enhancement in the stacked hole array is concentrated in the space between the metal sheets that lies between the holes, in agreement with previous work.[29] In summary, we have extended the use of localized surface-plasmon resonances in explaining the optical response of stacked particle-array structures to include stacked hole arrays, structures that are in essence the same as fishnet-type electromagnetic metamaterials. It is hoped that viewing electromagnetic metamaterials from the perspective of localized surface-plasmon resonances may enable concepts from plasmonics to be carried over into the metamaterials regime.

## ACKNOWLEDGMENTS

This work was supported through funding from Hewlett Packard (Bristol) in association with Great Western Research (http://www.gwr.ac.uk). W.L.B. has the pleasure of acknowledging the Royal Society for support through a Merit Award. E.H. acknowledges support from the EPSRC-GB and RCUK.

[1] V. G. Veselago, Sov. Phys. Usp. **10**, 509 (1968).
[2] J. B. Pendry, A. J. Holden, W. J. Stewart, and I. Youngs, Phys. Rev. Lett. **76**, 4773 (1996).
[3] J. B. Pendry, A. J. Holden, D. J. Robbins, and A. J. Stewart, IEEE Trans. Microwave Theory Tech. **47**, 2075 (1999).
[4] R. A. Shelby, D. R. Smith, and S. Schultz, Science **292**, 77 (2001).
[5] S. Zhang, W. Fan, N. C. Panoiu, K. J. Malloy, R. M. Osgood, and S. R. J. Brueck, Phys. Rev. Lett. **95**, 137404 (2005).
[6] G. Dolling, C. Enkrich, M. Wegener, J. F. Zhou, and C. M. Soukoulis, Opt. Lett. **30**, 3198 (2005).
[7] J. F. Zhou, T. Koschny, L. Zhang, G. Tuttle, and C. M. Soukoulis, Appl. Phys. Lett. **88**, 221103 (2006).
[8] V. A. Fedotov, P. L. Mladyonov, S. L. Prosvirnin, and N. I. Zheludev, Phys. Rev. E **72**, 056613 (2005).
[9] G. Dolling, C. Enkrich, M. Wegener, C. M. Soukoulis, and S.

Linden, Science **312**, 892 (2006).
[10] N. Engheta, Science **317**, 1698 (2007).
[11] J. Valentine, S. Zhang, T. Zentgraf, E. Ulin-Aula, D. A. Genov, G. Bartal, and X. Zhang, Nature (London) **455**, 376 (2008).
[12] G. Dolling, M. Wegener, C. M. Soukoulis, and S. Linden, Opt. Lett. **32**, 53 (2007).
[13] A. Christ, T. Zentgraf, S. G. Tikhodeev, N. A. Gippius, O. J. F. Martin, J. Kuhl, and H. Giessen, Phys. Status Solidi B **243**, 2344 (2006).
[14] E. Hutter and J. H. Fendler, Adv. Mater. **16**, 1685 (2004).
[15] W. A. Murray and W. L. Barnes, Adv. Mater. **19**, 3771 (2007).
[16] J. Prikulis, P. Hanarp, L. Olofsson, D. Sutherland, and M. Käll, Nano Lett. **4**, 1003 (2004).
[17] C. Sonnichsen, A. C. Duch, G. Steininger, M. Koch, G. von Plessen, and J. Feldmann, Appl. Phys. Lett. **76**, 140 (2000).
[18] J. Parsons, E. Hendry, C. P. Burrows, B. Auguié, J. R. Sambles, and W. L. Barnes, Phys. Rev. B **79**, 073412 (2009).
[19] T. V. Teperik, F. J. Garcia de Abajo, A. G. Borisov, M. Abdelsah, P. N. Bartlett, Y. Sugwara, and J. J. Baumberg, Nat. Photonics **2**, 299 (2008).
[20] E. D. Palik, *Handbook of Optical Constants of Solids* (Academic, New York, 1985).
[21] B. Auguié and W. L. Barnes, Phys. Rev. Lett. **101**, 143902 (2008).
[22] T. W. Ebbesen, H. J. Lezec, H. F. Ghaemi, T. Thio, and P. A. Wolff, Nature (London) **391**, 667 (1998).
[23] C. Haynes, A. D. McFarland, L. Zhao, R. P. Van Duyne, G. C. Schatz, L. Gunnarsson, J. Prikulis, B. Kasemo, and M. Kall, J. Phys. Chem. B **107**, 7337 (2003).
[24] W. A. Murray, B. Auguie, and W. L. Barnes, J. Phys. Chem. C **113**, 5120 (2009).
[25] L. H. Smith, M. C. Taylor, I. R. Hooper, and W. L. Barnes, J. Mod. Opt. **55**, 2929 (2008).
[26] D. Sarid, Phys. Rev. Lett. **47**, 1927 (1981).
[27] W. Rechberger, A. Hohenau, A. Leitner, J. R. Krenn, B. Lamprecht, and F. R. Aussenegg, Opt. Commun. **220**, 137 (2003).
[28] N. Liu, H. Guo, S. Kaiser, H. Schweizer, and H. Giessen, Nature Mater. **7**, 31 (2008).
[29] A. Mary, S. G. Rodrigo, F. J. Garcia-Vidal, and L. Martin-Moreno, Phys. Rev. Lett. **101**, 103902 (2008).
[30] J. Yao, Z. Liu, Y. Liu, Y. Wang, C. Sun, G. Bartal, A. M. Stacy, and X. Zhang, Science **321**, 930 (2008).
[31] D. R. Smith, S. Schultz, P. Markos, and C. M. Soukoulis, Phys. Rev. B **65**, 195104 (2002).
[32] R. A. Depine and A. Lakhtakia, Microwave Opt. Technol. Lett. **41**, 315 (2004).
[33] S. Zhang, Y.-S. Park, J. Li, X. Lu, W. Zhang, and X. Zhang, Phys. Rev. Lett. **102**, 023901 (2009).
[34] T. Koschny, P. Markos, D. R. Smith, and C. M. Soukoulis, Phys. Rev. E **68**, 065602(R) (2003).
[35] A. V. Kildishev, W. Cai, U. D. Chettiar, H.-S. Yuan, A. K. Sarychev, V. P. Drachev, and V. M. Shalaev, J. Opt. Soc. Am. B **23**, 423 (2006).
[36] C. Imhof and R. Zengerle, Appl. Phys. A **94**, 45 (2009).